Cooperative AF-based 3D Mobile UAV Relaying for Hybrid Satellite-Terrestrial Networks

Pankaj K. Sharma*, Deepika Gupta†, and Dong In Kim‡
*Department of Electronics and Communication Engineering, National Institute of Technology Rourkela, Odisha, India
†Department of Electronics and Communication Engineering,
Dr S P M International Institute of Information Technology, Naya Raipur, Chhattisgarh, India
‡Department of Electrical and Computer Engineering, Sungkyunkwan University, Suwon, South Korea
Email: sharmap@nitrkl.ac.in, deepika@iiitnr.edu.in, dikim@skku.ac.kr

***Abstract*—In this paper, we consider a hybrid satellite-terrestrial network (HSTN) where a multiantenna satellite communicates with a ground user equipment (UE) with the help of multiple amplify-and-forward (AF) three-dimensional (3D) mobile unmanned aerial vehicle (UAV) relays. Herein, we employ a stochastic mixed mobility (MM) model to deploy mobile UAV relays in a 3D cylindrical cell with UE at its ground centre. Taking into account the multiantenna satellite links and the random 3D distances between UAV relays and UE, we analyze the outage probability (OP) of considered system under an opportunistic UAV relay selection policy. We further carry out asymptotic OP analysis to present insights on system diversity order. Moreover, we compare the performance of proposed 3D mobile UAV relaying with the fixed altitude mobile UAV relaying as well as the fixed distance static relaying schemes. The analysis will be verified through simulations.**

I. Introduction

Cooperative relaying integration to satellite communication to mitigate the deleterious masking effect results in hybrid satellite-terrestrial network (HSTN) [1]. In HSTNs, the satellite and terrestrial link channels are modeled as Shadowed-Rician (SR) and Nakagami-*m* distributed. In [1]-[3], the performance of amplify-and-forward (AF)-based HSTNs has been investigated. Whereas, in [4], [5], the performance of decode-and-forward (DF)-based HSTNs has been analyzed. The common to all these works is the investigation with static relays without focusing on aerial mobile relays.

Unmanned aerial vehicles (UAVs) have recently been considered as aerial wireless access platforms for future communications [8]. The low cost and portability of the commercial UAVs qualify them as eligible candidates for aerial mobile relays. Backed by three-dimensional (3D) mobility and static hovering features, a rotary-wing type UAV is anticipated to be a readily deployable 3D mobile relay. In particular, in [9]-[10], the UAV has been employed as aerial mobile relay for terrestrial networks. Recently, in [11], a 3D mobility-based uplink UAV network has been analyzed. To our best knowledge, despite of innumerable advantages, the performance of 3D mobile UAV relaying for HSTNs has not been yet investigated. In general, such a performance analysis is complicated by the unavailability of concrete stochastic models for the characterization of 3D UAV movement process. An initiative to this end, we have most recently proposed a stochastic mixed mobility (MM) model for 3D UAV movement process in [12], [13], where a UAV makes vertical and horizontal transitions based on the random waypoint mobility (RWPM) and random walk (RW) mobility model, respectively. The MM model may be applied to UAV relays due to their random 3D locations under some control mechanisms, e.g., altitude, trajectory, etc. Note that the 3D mobility-based analysis is desirable, especially when the 3D point processes fail to yield a tractable analysis.

Motivated by the above, in this paper, we investigate the outage probability (OP) of an HSTN that comprises of a multiantenna satellite communicating with a ground receiver via multiple AF 3D mobile UAV relays under opportunistic relay selection. We also perform the asymptotic analysis to draw useful insights. Herein, we also take into account the fixed altitude mobile UAV relaying as well as fixed distance static relaying schemes for OP comparison with our 3D mobile UAV relaying scheme. In both cases, the proposed 3D mobile UAV relaying will be shown to yield better performance.

Notations: $\mathbb{E}[\cdot]$ represents the statistical expectation. $\|\cdot\|$ denotes the Euclidean norm. The acronyms pdf and cdf stand for probability density function $f_X(\cdot)$ and cumulative distribution function $F_X(\cdot)$ of random variable X, respectively.

II. System Description

A. System Model

We consider an HSTN where a satellite S equipped with N antennas communicates with a single-antenna ground UE D via M single-antenna 3D UAV relays U_i, $i \in \{1, ..., M\}$. Here, at any time t, we assume that the UAVs make 3D spatial transitions based on MM model [12], [13]. The instantaneous altitude of a UAV U_i at time t is denoted by $h_i(t)$ whereas the spatial location is represented as $z_i(t)$. While the UAVs operate in a 3D cylindrical region of radius R and height H above the ground plane, the UE D is located at the centre of the base of this cylindrical region. Moreover, we consider that the aforementioned cylindrical region lies beneath the circular spot beam of satellite S centered around the UE D. We consider that no co-channel interferers are present[1] to influence the signal reception at D. All UAVs can update their 3D locations in discrete time slots. The channel vector from S to U_i is denoted as $\mathbf{g}_{su_i} \in \mathbb{C}^{1\times N}$ and the channel between U_i and D is denoted as $\mathrm{g}_{u_i d}$. We assume all the receiving nodes are inflicted by the additive white Gaussian noise (AWGN) with zero mean and variance σ^2.

[1]The more generalized case of co-channel interference may be deferred to future works.

978-1-7281-5207-3/20/$31.00 ©2020 IEEE

B. Mixed Mobility Model for 3D UAV Movement Process

In MM model [12], [13], at time t, a UAV ascends/descends in vertical direction based on the RWPM model with random dwell time at each waypoint. During this dwell time, the UAV goes for a spatial excursion by following the RW mobility model. Let, the instantaneous altitude $h_i(t)$ of UAV as uniformly random in interval $[0, H]$, the vertical velocity $v_{1,i}(t)$ at waypoints is uniformly random in interval $[v_{min}, v_{max}]$, where v_{min} and v_{max} represent, respectively, the minimum and maximum speeds. T_s denotes the uniform random dwell time in interval $[\tau_{min}, \tau_{max}]$. Letting p_s as the staying probability at waypoints, the pdf of instantaneous altitude $h_i(t)$ is formulated by the superposition of a static and a mobility pdfs as

$$f_{h_i}(x|t) = p_\mathrm{s} f^{st}_{h_i}(x|t) + (1-p_\mathrm{s}) f^{mo}_{h_i}(x|t), \tag{1}$$

where $f^{st}_{h_i}(x|t) = \frac{1}{H}$ and $f^{mo}_{h_i}(x|t) = -\frac{6x^2}{H^3} + \frac{6x}{H^2}$, for $0 \leq x \leq H$, with $p_\mathrm{s} = \frac{\mathbb{E}[T_\mathrm{s}]}{\mathbb{E}[T_\mathrm{s}]+\mathbb{E}[T_\mathrm{m}]}$ involving $\mathbb{E}[T_\mathrm{s}]$ as the mean stay time and $\mathbb{E}[T_\mathrm{m}] = \frac{\ln(v_{max}/v_{min})}{v_{max}-v_{min}} \frac{H}{3}$ as the mean vertical movement time.

Moreover, in a discrete time slot beginning at t during dwell time T_s, the spatial transition is made with probability p_s as

$$z_i(t+1) = z_i(t) + \mathrm{u}_i(t), \tag{2}$$

where $\mathrm{u}_i(t)$ is uniform in ball $B(z_i(t), R')$ with R' as the maximum spatial mobility range. A previous spatial location of UAV can be retained as $z_i(t+1) = z_i(t)$ with probability $1-p_\mathrm{s}$. Let $v_{2,i}(t) = \|z_i(t) - z_i(t-1)\|$ is the velocity of spatial excursion, we have its mean value $\mathbb{E}[v_{2,i}(t)] = \mathbb{E}[\|z_i(t) - z_i(t-1)\|] = \frac{R'}{1.5}$. Hence, at time t, the pdf of distance $Z_i(t) = \|z_i(t)\|$ can be given by

$$f_{Z_i}(z|t) = \frac{2z}{R^2}, 0 \leq z \leq R. \tag{3}$$

It is worth mentioning that the wide variety of practical UAV movement scenarios can be generated by adjusting the parameters of the MM mobility model for UAVs.

C. Channel Models

1) Satellite Channel: The channel vector $\mathbf{g}_{su_i}$ whose entries follow uncorrelated independent and identically distributed (i.i.d.) SR fading can be modeled as $\mathbf{g}_{su_i} = \bar{\mathbf{g}}_{su_i} + \tilde{\mathbf{g}}_{su_i}$. Here, $\bar{\mathbf{g}}_{su_i}$ corresponds to LOS component with i.i.d. Nakagami-*m* distributed random variable with m_{su} and Ω_{su} as fading severity and average power, respectively. The entries of $\tilde{\mathbf{g}}_{su_i}$ are i.i.d. complex Gaussian random variable with zero mean and variance $2\flat_{su}$. For integer m_{su}, the probability density function (pdf) of norm $||\mathbf{g}_{su_i}||^2$ is given by [3]

$$f_{||\mathbf{g}_{su_i}||^2}(x) = \sum_{i_1=0}^{m_{su}-1} \cdots \sum_{i_N=0}^{m_{su}-1} \Xi(N) x^{\gamma-1} \mathrm{e}^{-(\beta_u - \delta_u)x}, \tag{4}$$

where $\alpha_u = (2\flat_{su} m_{su}/(2\flat_{su} m_{su} + \Omega_{su}))^{m_{su}}/2\flat_{su}$, $\beta_u = 1/2\flat_{su}$, and $\delta_u = \Omega_{su}/(2\flat_{su})(2\flat_{su} m_{su} + \Omega_{su})$, $\zeta(\kappa) = (-1)^\kappa (1-m_{su})_\kappa \delta_u^\kappa/(\kappa!)^2$, $(\cdot)_\kappa$ is the Pochhammer symbol [14, p. xliii], $\Xi(N) = \alpha_u^N \prod_{\kappa=1}^N \zeta(i_\kappa) \prod_{j=1}^{N-1} \mathcal{B}(\sum_{l=1}^j i_l + j, i_{j+1}+1)$, $\gamma = \sum_{\kappa=1}^N i_\kappa + N$, and $\mathcal{B}(.,.)$ denotes the Beta function [14, eq. 8.384.1].

Further, the instantaneous free space loss for satellite links can be computed as [7] $\mathcal{L}_{su_i}(t) = \frac{1}{\mathcal{K}_\mathcal{B}\mathcal{T}\mathcal{W}} \left(\frac{c}{4\pi f_\mathrm{c} \mathrm{d}_i(t)}\right)^2$, where $\mathcal{K}_\mathcal{B} = 1.38 \times 10^{-23}$J/K is the Boltzman constant, $\mathcal{T}$ is the receiver noise temperature, $\mathcal{W}$ is the carrier bandwidth, c is the speed of light, f_c is the carrier frequency, and $\mathrm{d}_i(t)$ is the distance[2] between the nodes S and U_i.

Also, the beam gain $\vartheta(\theta_i)$ of satellite can be expressed as $\vartheta(\theta_i) = \vartheta_i \left(\frac{\mathcal{J}_1(\rho_i)}{2\rho_i} + 36\frac{\mathcal{J}_3(\rho_i)}{\rho_i^3}\right)$,where θ_i is the angular separation[3] of node U_i from the satellite beam center, ϑ_i is the antenna gain at node U_i, $\mathcal{J}_\varrho(\cdot)$, $\varrho \in \{1,3\}$ is the Bessel function, and $\rho_i = 2.07123\frac{\sin\theta_i}{\sin\theta_{i3\mathrm{dB}}}$ with $\theta_{i3\mathrm{dB}}$ as 3dB beamwidth.

2) UAV Relay-to-Ground Channel: The terrestrial links between UAV relays U_i and destination D are assumed to follow Nakagami-*m* fading. Thus, the pdf of the channel gains $|g_{u_i d}|^2$ belongs to gamma distribution

$$f_{|g_{u_i d}|^2}(x) = \left(\frac{m_{ud}}{\Omega_{ud}}\right)^{m_{ud}} \frac{x^{m_{ud}-1}}{\Gamma(m_{ud})} \mathrm{e}^{-\frac{m_{ud}}{\Omega_{ud}}x}, \tag{5}$$

where m_{ud} and Ω_{ud} represent an integer-valued fading severity parameter and average channel power, respectively. Moreover, the instantaneous free-space path loss from UAV U_i to destination D can be expressed as

$$w_{id}^{-\alpha}(t) = \left(h_i^2(t) + Z_i^2(t)\right)^{-\frac{\alpha}{2}}, \tag{6}$$

where w_{id} is the distance from U_i to D, $Z_i(t) = \|z_i(t)\|$, and α is the path loss exponent.

D. Propagation Model

The communication from satellite S to destination D takes place in two consecutive time phases based on variable-gain AF relay cooperation. In the first phase, at time t, S beamforms its signal $x_s(t)$ (satisfying $\mathbb{E}[|x_s(t)|^2] = 1$) to UAV relay U_i. Thus, the received signal at U_i can be given by

$$y_{u_i}(t) = \sqrt{P_s \mathcal{L}_{su_i}(t) \vartheta_s \vartheta(\theta_{u_i})} \mathbf{g}_{su_i} \mathbf{w}_{su_i} x_s(t) + \nu_{u_i}, \tag{7}$$

where $\mathbf{w}_{su_i} = \frac{\mathbf{g}_{su_i}}{||\mathbf{g}_{su_i}||}$, ϑ_s denotes the satellite antenna gain, ν_{u_i} represents AWGN at D with variance σ^2.

In the second phase, at time $t+1$, the UAV relay U_i amplifies and forwards the received signal $y_{u_i}(t)$ with a gain factor to destination D which is given by

$$G = \sqrt{\frac{1}{P_s \mathcal{L}_{su_i}(t) \vartheta_s \vartheta(\theta_{u_i}) ||\mathbf{g}_{su_i}||^2 + \sigma^2}}. \tag{8}$$

Thus, the received signal at D can be expressed as

$$y_{id}(t+1) = \sqrt{P_u} w_{id}^{-\frac{\alpha}{2}}(t+1) G y_{u_i}(t) \mathrm{g}_{u_i d} + \nu_d, \tag{9}$$

where ν_d is the AWGN at D with variance σ^2. Thus, from (9), the SNR at D in the second phase can be given as

$$\Lambda_{id}(t+1) = \frac{\Lambda_{su_i}(t)\Lambda_{u_i d}(t+1)}{\Lambda_{su_i}(t) + \Lambda_{u_i d}(t+1) + 1}, \tag{10}$$

where $\Lambda_{su_i}(t) = \frac{P_s \mathcal{L}_{su_i}(t) \vartheta_s \vartheta(\theta_{u_i}) ||\mathbf{g}_{su_i}||^2}{\sigma^2}$ and $\Lambda_{u_i d}(t+1) = \frac{P_u w_{id}^{-\alpha}(t+1) |\mathrm{g}_{u_i d}|^2}{\sigma^2}$.

[2]Typically, the distance $\mathrm{d}_i(t)$ is very large (e.g., 35,786 Km, for geostationary (GEO) satellite), it may be approximately the same for all i. Hence, in this work, it is assumed to be deterministic for a tractable analysis.

[3]Likewise, under large distance from GEO satellite to UAV relays, the angular separation θ_i, ρ_i, and ϑ_i may be assumed the same for all i.

E. Relay Selection Policy

In this work, an opportunistic relay selection policy is implemented based on maximizing the SNR at D i.e.,

$$i^*(t) = \arg \max_{i \in 1,\ldots,M} \Lambda_{id}(t), t > 1. \tag{11}$$

As such, the relay selection policy in (11) is considered to minimize the system outage probability. Here, we assume that perfect channel state information (CSI) is available at central controller to implement the relay selection policy. Further, the frequency offset from Doppler effect is assumed to be either perfectly compensated or negligible under the slow movement speed of UAV relays. This assumption is widely considered in the previous works on HSTNs

III. OP with 3D Mobile UAV Relays

In this section, we determine the OP and asymptotic OP for the deployment of 3D mobile UAV relays using MM model. Note that both the altitude and spatial locations are variable in this case. Further, we drop the time notation t to focus on the OP analysis to realize one snapshot for causal S to D transmission (i.e., $t > 1$).

1) OP: With relay selection under independent and identically distributed (i.i.d.) SNRs Λ_{id}, $\forall i$, the OP of HSTN for a threshold γ_{th} can be given by

$$\mathcal{P}_{\text{out}}(\gamma_{\text{th}}) = [\Psi(\gamma_{\text{th}})]^M, \tag{12}$$

where the term $\Psi(\gamma_{\text{th}})$ is evaluated as

$$\begin{aligned}\Psi(\gamma_{\text{th}}) &= \Pr\left[\Lambda_{id} < \gamma_{\text{th}}\right] \\ &= 1 - \int_0^\infty \left[1 - F_{\Lambda_{su_i}}\left(\frac{\gamma_{\text{th}}(x+\gamma_{\text{th}}+1)}{x}\right)\right] \\ &\times f_{\Lambda_{u_id}}(x+\gamma_{\text{th}})dx.\end{aligned} \tag{13}$$

In (13), the cumulative distribution function (cdf) $F_{\Lambda_{su_i}}(x)$ can be evaluated based on the pdf in (4) after a variable transformation $\Lambda_{su_i} = \eta_u ||\mathbf{g}_{su_i}||^2$ as

$$\begin{aligned}F_{\Lambda_{su_i}}(x) = 1 - \sum_{i_1=0}^{m_{su}-1} \cdots \sum_{i_N=0}^{m_{su}-1} \frac{\Xi(N)}{(\eta_u)^\gamma} \sum_{p=0}^{\gamma-1} \frac{(\gamma-1)!}{p!} \\ \times \Theta_u^{-(\gamma-p)} x^p \mathrm{e}^{-\Theta_u x}.\end{aligned} \tag{14}$$

where $\Theta_u = \frac{\beta_u - \delta_u}{\eta_u}$ and $\eta_u = \frac{P_s \mathcal{L}_{su} \vartheta_s \vartheta(\theta_u)}{\sigma^2}$.

As opposed to the static relays, the mobile UAV relays U_i occupy random locations in 3D region, and thus, the distance w_{id} between U_i and D is random. Considering W_{id} as the random variable, its pdf for MM model is given as [13]

$$f_{W_{id}}(w) = p_{\text{s}} f^{st}_{W_{id}}(w) + (1 - p_{\text{s}}) f^{mo}_{W_{id}}(w), \tag{15}$$

where the weight p_s is the staying probability of UAV at waypoints, $f^{st}_{W_{id}}(w)$ is the pdf of W_{id} if UAV U_i makes the horizontal transition, and $f^{mo}_{W_{id}}(w)$ is the pdf of W_{id} if UAV U_i makes the vertical ascent/descent, and are expressed as

$$f^{st}_{W_{id}}(w) = \begin{cases} \frac{2w^2}{R^2 H}, \text{ for } 0 \le w < H, \\ \frac{2w}{R^2}, \text{ for } H \le w < R, \\ \frac{2w}{R^2} - \frac{2w\sqrt{w^2-R^2}}{R^2 H}, \\ \qquad \text{for } R \le w \le \sqrt{R^2+H^2}, \end{cases} \tag{16}$$

and

$$f^{mo}_{W_{id}}(w) = \begin{cases} \frac{6w^3}{R^2H^2} - \frac{4w^4}{R^2H^3}, \text{ for } 0 \le w < H, \\ \frac{2w}{R^2}, \text{ for } H \le w < R, \\ \frac{2w}{R^2} - \frac{6w(w^2-R^2)}{R^2H^2} + \frac{4w(w^2-R^2)^{\frac{3}{2}}}{R^2H^3}, \\ \qquad \text{for } R \le w \le \sqrt{R^2+H^2}. \end{cases} \tag{17}$$

Further, we derive the pdf $f_{\Lambda_{u_id}}(x) = \frac{d}{dx} F_{\Lambda_{u_id}}(x)$, where

$$\begin{aligned}F_{\Lambda_{u_id}}(x) &= \Pr\left[\eta'_u W_{id}^{-\alpha} |g_{u_id}|^2 < x\right] \\ &= \int_0^{\sqrt{R^2+H^2}} \frac{\Upsilon\left(m_{ud}, \frac{m_{ud}x}{\Omega_{ud}\eta'_u} r^\alpha\right)}{\Gamma(m_{ud})} f_{W_{id}}(r)dr,\end{aligned} \tag{18}$$

with $\eta'_u = \frac{P_u}{\sigma^2}$. After taking a derivative, we can get the pdf

$$\begin{aligned}f_{\Lambda_{u_id}}(x) = \frac{1}{\Gamma(m_{ud})} \left(\frac{m_{ud}}{\Omega_{ud}\eta'_u}\right)^{m_{ud}} x^{m_{ud}-1} \\ \times \int_0^{\sqrt{R^2+H^2}} r^{m_{ud}\alpha} \mathrm{e}^{-\frac{m_{ud}x}{\Omega_{ud}\eta'_u} r^\alpha} f_{W_{id}}(r)dr.\end{aligned} \tag{19}$$

Next, we invoke (14) and (19) in (13), to get $\Psi(\gamma_{\text{th}})$ as shown in (20) at the top of next page, where $\mathcal{K}_v(\cdot)$ denotes the vth order Bessel function of second kind [14]. Note that the derived expression can be readily computed numerically by mathematical softwares.

2) Asymptotic OP: To gain insights, we simplify the previous OP expressions at high SNR ($P_s, P_u \to \infty$). At high SNR, we invoke $\Lambda_{id} \le \min(\Lambda_{su_i}, \Lambda_{u_id})$ in (13) and neglect the higher-order product of cdf term from the resulting analysis to achieve

$$\mathcal{P}_{\text{out}}(\gamma_{\text{th}}) \simeq \left[F_{\Lambda_{su_i}}(\gamma_{\text{th}}) + F_{\Lambda_{u_id}}(\gamma_{\text{th}})\right]^M. \tag{21}$$

For uncorrelated fading, we can have the simplified cdf $F_{\Lambda_{su_i}}(x)$ under small x as [3]

$$F_{\Lambda_{su_i}}(x) \simeq \frac{\alpha_u^N x^N}{N! \eta_u^N}. \tag{22}$$

Further, by applying the approximation $\Upsilon(\upsilon, x) \simeq \frac{x^\upsilon}{\upsilon}$, for small x, the cdf in (18) can be simplified as

$$\begin{aligned}F_{\Lambda_{u_id}} \simeq \frac{1}{m_{ud}!} \left(\frac{m_{ud}x}{\Omega_{ud}\eta'_u}\right)^{m_{ud}} \\ \times \int_0^{\sqrt{R^2+H^2}} r^{m_{ud}\alpha} f_{W_{id}}(r)dr.\end{aligned} \tag{23}$$

Finally, on substituting the cdf given by (23) into (21), the asymptotic OP can be given by (24) at the top of next page.

IV. OP with Fixed Altitude Mobile UAV Relays

In this section, we consider another variant of 3D mobile UAV relaying where UAV relays are deployed at a fixed altitude H of the considered cylindrical region of radius R. Specifically, we assume that the UAVs can make transitions in a circular disk region at height H based on the RW mobility model only. Therefore, at any time t, the spatial transitions by UAVs can be described by the same expression as in (2). Consequently, the distribution of UAV relays remains uniform in the resulting circular disk region at height H. For this special case, the instantaneous free-space path loss from UAV U_i to destination D can be expressed as

$$w_{id}^{-\alpha}(t) = \left(H^2 + Z_i^2(t)\right)^{-\frac{\alpha}{2}}, \tag{25}$$

$$\Psi(\gamma_{\text{th}}) = 1 - \sum_{i_1=0}^{m_{su}-1} \cdots \sum_{i_N=0}^{m_{su}-1} \frac{\Xi(N)}{(\eta_u)^{\gamma}} \sum_{p=0}^{\gamma-1} \frac{(\gamma-1)!}{p!} \sum_{q=0}^{p} \binom{p}{q} \mathrm{e}^{-\Theta_u \gamma_{\text{th}}} \sum_{n=0}^{m_{ud}-1} \binom{m_{ud}-1}{n} \tag{20}$$
$$\times \frac{2}{\Gamma(m_{ud})} \left(\frac{m_{ud}}{\Omega_{ud}\eta'_u}\right)^{m_{ud}-\frac{n-q+1}{2}} \Theta_u^{\frac{n-q+1}{2}-(\gamma-p)} \gamma_{\text{th}}^{m_{ud}+p-\frac{n+q+1}{2}} (\gamma_{\text{th}}+1)^{\frac{n+q+1}{2}}$$
$$\times \left[\int_0^H r^{\left(m_{ud}-\frac{n-q+1}{2}\right)\alpha} \mathrm{e}^{-\frac{m_{ud}\gamma_{\text{th}} r^{\alpha}}{\Omega_{ud}\eta'_u}} \mathcal{K}_{n-q+1}\left(2\sqrt{\Theta_u \gamma_{\text{th}}(\gamma_{\text{th}}+1)\frac{m_{ud}\gamma_{\text{th}} r^{\alpha}}{\Omega_{ud}\eta'_u}}\right) \right.$$
$$\left. \times \left[p_{\text{s}} \frac{2r^2}{R^2 H} + (1-p_{\text{s}}) \left(\frac{6r^3}{R^2H^2} - \frac{4r^4}{R^2H^3}\right) \right] dr \right.$$
$$+ \int_H^R r^{\left(m_{ud}-\frac{n-q+1}{2}\right)\alpha} \mathrm{e}^{-\frac{m_{ud}\gamma_{\text{th}} r^{\alpha}}{\Omega_{ud}\eta'_u}} \mathcal{K}_{n-q+1}\left(2\sqrt{\Theta_u \gamma_{\text{th}}(\gamma_{\text{th}}+1)\frac{m_{ud}\gamma_{\text{th}} r^{\alpha}}{\Omega_{ud}\eta'_u}}\right) \frac{2r}{R^2} dr$$
$$+ \int_R^{\sqrt{R^2+H^2}} r^{\left(m_{ud}-\frac{n-q+1}{2}\right)\alpha} \mathrm{e}^{-\frac{m_{ud}\gamma_{\text{th}} r^{\alpha}}{\Omega_{ud}\eta'_u}} \mathcal{K}_{n-q+1}\left(2\sqrt{\Theta_u \gamma_{\text{th}}(\gamma_{\text{th}}+1)\frac{m_{ud}\gamma_{\text{th}} r^{\alpha}}{\Omega_{ud}\eta'_u}}\right)$$
$$\left. \times \left[p_{\text{s}} \left(\frac{2r}{R^2} - \frac{2r\sqrt{r^2-R^2}}{R^2 H}\right) + (1-p_{\text{s}}) \left(\frac{2r}{R^2} - \frac{6r(r^2-R^2)}{R^2H^2} + \frac{4r(r^2-R^2)^{\frac{3}{2}}}{R^2H^3}\right) \right] dr \right].$$

$$\mathcal{P}_{\text{out}}(\gamma_{\text{th}}) \simeq \left[\frac{\alpha_u^N \gamma_{\text{th}}^N}{N! \eta_u^N} + \frac{1}{m_{ud}!} \left(\frac{m_{ud}\gamma_{\text{th}}}{\Omega_{ud}\eta'_u}\right)^{m_{ud}} \left[\int_0^H r^{m_{ud}\alpha} \left[p_{\text{s}} \frac{2r^2}{R^2 H} + (1-p_{\text{s}}) \left(\frac{6r^3}{R^2H^2} - \frac{4r^4}{R^2H^3}\right) \right] dr + \int_H^R r^{m_{ud}\alpha} \frac{2r}{R^2} dr \right. \right. \tag{24}$$
$$\left. \left. + \int_R^{\sqrt{R^2+H^2}} r^{m_{ud}\alpha} \left[p_{\text{s}} \left(\frac{2r}{R^2} - \frac{2r\sqrt{r^2-R^2}}{R^2 H}\right) + (1-p_{\text{s}}) \left(\frac{2r}{R^2} - \frac{6r(r^2-R^2)}{R^2H^2} + \frac{4r(r^2-R^2)^{\frac{3}{2}}}{R^2H^3}\right) \right] dr \right] \right]^M.$$

$$\Psi(\gamma_{\text{th}}) = 1 - \sum_{i_1=0}^{m_{su}-1} \cdots \sum_{i_N=0}^{m_{su}-1} \frac{\Xi(N)}{(\eta_u)^{\gamma}} \sum_{p=0}^{\gamma-1} \frac{(\gamma-1)!}{p!} \sum_{q=0}^{p} \binom{p}{q} \mathrm{e}^{-\Theta_u \gamma_{\text{th}}} \sum_{n=0}^{m_{ud}-1} \binom{m_{ud}-1}{n} \tag{27}$$
$$\times \frac{2}{\Gamma(m_{ud})} \left(\frac{m_{ud}}{\Omega_{ud}\eta'_u}\right)^{m_{ud}-\frac{n-q+1}{2}} \Theta_u^{\frac{n-q+1}{2}-(\gamma-p)} \gamma_{\text{th}}^{m_{ud}+p-\frac{n+q+1}{2}} (\gamma_{\text{th}}+1)^{\frac{n+q+1}{2}}$$
$$\times \int_H^{\sqrt{R^2+H^2}} r^{\left(m_{ud}-\frac{n-q+1}{2}\right)\alpha} \mathrm{e}^{-\frac{m_{ud}\gamma_{\text{th}} r^{\alpha}}{\Omega_{ud}\eta'_u}} \mathcal{K}_{n-q+1}\left(2\sqrt{\Theta_u \gamma_{\text{th}}(\gamma_{\text{th}}+1)\frac{m_{ud}\gamma_{\text{th}} r^{\alpha}}{\Omega_{ud}\eta'_u}}\right) \frac{2r}{R^2} dr.$$

where H is the same for all UAV relays. Note that the pdf of $Z_i(t)$ for this case is the same as given by (3) previously. Hence, in one snapshot, the pdf of W_{id} can be calculated as

$$f_{W_{id}}(w) = \begin{cases} \frac{2w}{R^2}, \text{ for } H \le w \le \sqrt{R^2+H^2}, \\ 0, \text{ else.} \end{cases} \tag{26}$$

1) OP: The OP for this case can be computed based on (12) where the function $\Psi(\gamma_{\text{th}})$ is evaluated by invoking the pdf in (26) as (27) at the top of this page.

2) Asymptotic OP: Likewise, we can evaluate the asymptotic OP based on (21) using (22) and (23), where in (23), the pdf in (26) is invoked. Finally, the asymptotic OP for this case can be expressed as

$$\mathcal{P}_{\text{out}}(\gamma_{\text{th}}) \simeq \left[\frac{\alpha_u^N \gamma_{\text{th}}^N}{N! \eta_u^N} + \frac{2}{m_{ud}!} \left(\frac{m_{ud}\gamma_{\text{th}}}{\Omega_{ud}\eta'_u}\right)^{m_{ud}} \times \int_H^{\sqrt{R^2+H^2}} r^{m_{ud}\alpha} \frac{2r}{R^2} dr \right]^M. \tag{28}$$

Remark: For $\eta_u = \eta'_u = \eta$, by observing the exponent of term η in asymptotic OP expressions given by (24) and (28) for the proposed 3D mobile UAV relaying and fixed altitude mobile UAV relaying, respectively, we can deduce the diversity order of the system as $M \min(N, m_{ud})$. Note that the achievable diversity order of the system remains unaffected by the choice of these mobile UAV relaying schemes.

V. Numerical Results

We set satellite parameters using [7] as $\mathcal{T} = 300$ K, $\mathcal{W} = 15$ MHz, $c = 3 \times 10^8$ m/s, $\mathrm{d}_i = 35,786$ Km, $f_{\text{c}} = 2$ GHz, $\vartheta_i = 4.8$ dB, $\vartheta_s = 53.45$ dB, $\theta_i = 0.8°$, $\theta_{i3\text{dB}} = 0.3°$, and $(m_{su}, \flat_{su}, \Omega_{su}) = (2, 0.063, 0.0005)$ for heavy shadowing. For UAVs, we set the parameters as $v_{1,i} \sim [0.1, 30]$ m/s, $v_{2,i} \sim [0, 40]$ m/s, $H = 40$ m, $R = 80$ m, $\Omega_{ud} = 1$, and $\alpha = 2$. Here, $p_{\text{s}} = 0.5$ is set by adjusting the distribution of dwell time duration T_{s}. We also set $\eta_u = \eta'_u = \eta$ and $\gamma_{\text{th}} = 1$.

Fig. 1 plots the OP curves versus SNR for 3D mobile UAV relaying and fixed altitude mobile UAV relaying. Here, we can observe that the simulations and asymptotic analysis are well-aligned with the theoretical analysis. By observing the set of curves for $(M, N, m_{ud}) = (1, 2, 1)$, $(2, 2, 1)$, and $(2, 2, 2)$, we can verify the diversity order of $M \min(N, m_{ud})$ for both

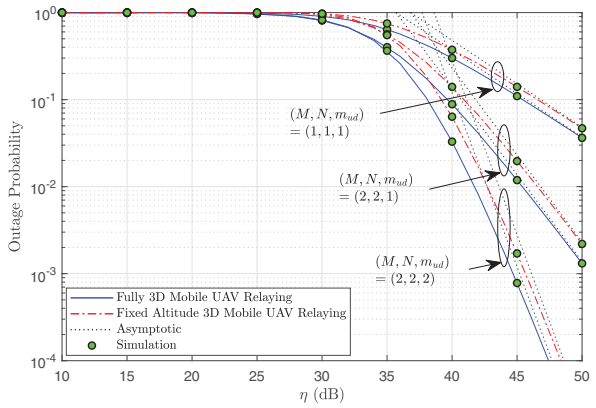

Fig. 1. OP comparison of 3D mobile UAV relaying with fixed altitude mobile UAV relaying.

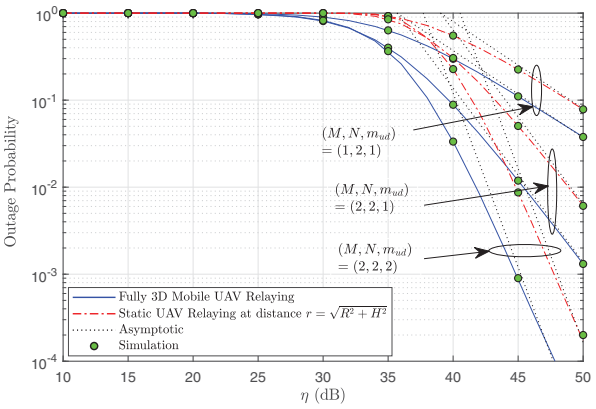

Fig. 2. OP comparison of 3D mobile UAV relaying with fixed distance static relaying.

the relaying schemes. Clearly, the 3D mobile UAV relaying provides better performance as compared to the fixed altitude mobile UAV relaying.

Fig. 2 plots the OP curves versus SNR for 3D mobile UAV relaying and fixed distance UAV relaying. For comparison with fixed distance static relaying, we locate the relays at a fixed distance $\sqrt{R^2 + H^2}$ from D. As such, it represents the maximum dynamic range of distance of UAV relays from UE. For this case, the OP can be calculated using $\Psi(\gamma_{\text{th}})$ in (12) based on setting $r = \sqrt{R^2 + H^2}$ in the underlying pdf $f_{\Lambda_{u_i d}}(x)$ in (19) and neglecting the final integral over the pdf $f_{W_{id}}(r)$. Here, we can see that the simulations and asymptotic analysis conform to our theoretical analysis. From the set of curves for $(M, N, m_{ud}) = (1, 2, 1)$, $(2, 2, 1)$, and $(2, 2, 2)$, the diversity order of $M \min(N, m_{ud})$ can be readily verified for both the relaying schemes. Apparently, the 3D mobile UAV relaying outperforms the fixed distance static relaying.

VI. Conclusion

We have evaluated the OP of an HSTN having multiantenna satellite communication with a ground UE via multiple AF 3D mobile UAV relays under an opportunistic UAV relay selection policy. We have considered the fixed altitude mobile UAV relaying as well as the fixed distance static relaying schemes to compare their OP performance with the proposed 3D mobile UAV relaying scheme. We have shown that the proposed 3D mobile UAV relaying scheme is advantageous over the fixed altitude mobile UAV relaying and fixed distance static relaying schemes, especially if (a) the UAVs are deployed at a height H above the ground plane in the former scheme; (b) the static relays are deployed at the maximum dynamic range of UAVs' distance in the latter scheme.

VII. Acknowledgement

This work was supported in part by the National Research Foundation of Korea (NRF) Grant funded by the Korean Government under Grant 2017R1A2B2003953. This work was supported in part by the Science and Engineering Research Board, Department of Science and Technology, Govt. of India (Project no. SRG/2019/000979).

References

[1] M. R. Bhatnagar and Arti M. K., "Performance analysis of AF based hybrid satellite-terrestrial cooperative network over generalized fading channels," *IEEE Commun. Lett.*, vol. 17, no. 10, pp. 1912-1915, Oct. 2013.

[2] K. An, M. Lin, and T. Liang "On the performance of multiuser hybrid satellite-terrestrial relay networks with opportunistic scheduling," *IEEE Commun. Lett.*, vol. 19, no. 10, pp. 1722-1725, Oct. 2015.

[3] P. K. Upadhyay and P. K. Sharma, "Max-max user-relay selection scheme in multiuser and multirelay hybrid satellite-terrestrial relay systems," *IEEE Commun. Lett.*, vol. 20, no. 2, pp. 268-271, Feb. 2016.

[4] S. Sreng, B. Escrig, M.-L. Boucheret, "Exact symbol error probability of hybrid/integrated satellite-terrestrial cooperative network," *IEEE Trans. Wireless Commun.*, vol. 12, no. 3, pp. 1310-1319, Mar. 2013.

[5] K. An, M. Lin, J. Ouyang, Y. Huang, and G. Zheng, "Symbol error analysis of hybrid satellite-terrestrial cooperative networks with co-channel interference," *IEEE Commun. Lett.*, vol. 18, no. 11, pp. 1947-1950, Nov. 2014.

[6] P. K. Sharma, P. K. Upadhyay, D. B. da Costa, P. S. Bithas, and A. G. Kanatas, "Performance analysis of overlay spectrum sharing in hybrid satellite-terrestrial systems with secondary network selection," *IEEE Trans. Wireless Commun.*, vol. 16, no. 10, pp. 6586-6601, Oct. 2017.

[7] K. Guo, K. An, B. Zhang, Y. Huang, and G. Zheng, "Outage analysis of cognitive hybrid satellite-terrestrial networks with hardware impairments and multi-primary user," *IEEE Wireless Commun. Lett.*, vol. 7, no. 5, pp. 816-819, Apr. 2018.

[8] M. Mozaffari, W.Saad, M.Bennis, Y. -H. Nam, and M. Debbah "A tutorial on UAVs for wireless networks: Applications, challenges, and open problems," [Online]. Available: http://arxiv.org/abs/1803.00680.

[9] Y. Zeng, R. Zhang, and T. J. Lim "Throughput maximization for UAV-enabled mobile relaying systems," *IEEE Trans. Commun.*, vol. 64, no. 12, pp. 4983-4996, Dec. 2016.

[10] F. Ono, H. Ochiai, and R. Miura, "A wireless relay network based on unmanned aircraft system with rate optimization," *IEEE Trans. Wireless Commun.*, vol. 15, no. 11, pp. 7699-7708, Nov. 2016.

[11] M. Banagar and H. S. Dhillon, "Performance characterization of canonical mobility models in drone cellular networks," [Online]. Available:https://arxiv.org/abs/1908.05243. Accessed: March 2019.

[12] P. K. Sharma and D. I. Kim, "Coverage probability of 3-D mobile UAV networks," *IEEE Wireless Commun. Lett.*, vol. 8, no. 1, pp. 97-100, Feb. 2019.

[13] P. K. Sharma and D. I. Kim, "Random 3D mobile UAV networks: Mobility modeling and coverage probability," *IEEE Trans. Wireless Commun.*, vol. 18, no. 5, pp. 2527-2538, May 2019.

[14] I. S. Gradshteyn and I. M. Ryzhik, *Tables of Integrals, Series and Products*, 6th ed. New York: Academic Press, 2000.